

Predicting excited states from ground state wavefunction by supervised quantum machine learning

Hiroki Kawai*

*Electrical and Computer Engineering Department, Boston University,
8 Saint Marys Street, Boston, MA, United States, 02215*

Yuya O. Nakagawa†

QunaSys Inc., Aqua Hakusan Building 9F, 1-13-7 Hakusan, Bunkyo, Tokyo 113-0001, Japan

(Dated: April 19, 2022)

Excited states of molecules lie in the heart of photochemistry and chemical reactions. The recent development in quantum computational chemistry leads to inventions of a variety of algorithms which calculate the excited states of molecules on near-term quantum computers, but they require more computational burdens than the algorithms for the ground states. In this study, we propose a scheme of supervised quantum machine learning which predicts excited state properties of molecules only from its ground state wavefunction and results in reducing the computational cost for calculating the excited states. Our model is comprised of a quantum reservoir and a classical machine learning unit which processes the results of measurements of single-qubit Pauli operators. The quantum reservoir effectively transforms the single-qubit operators into complicated multi-qubit ones which contain essential information of the system, so that the classical machine learning unit may decode them appropriately. The number of runs for quantum computers is saved by training only the classical machine learning unit and the whole model requires modest resources of quantum hardwares which may be implemented in current experiments. We illustrate the predictive ability of our model by numerical simulations for small molecules with and without including noise inevitable in near-term quantum computers. The results show that our scheme well reproduces the first and second excitation energies as well as the transition dipole moment between the ground states and excited states only from the ground state as an input. Our contribution will enhance applications of quantum computers in the study of quantum chemistry and quantum materials.

I. INTRODUCTION

The rapid growth of the machine learning technology in the last decade has revealed its potential to be utilized in various engineering fields such as image recognition, natural language processing, and outlier detection [1, 2]. Its applications to scientific fields as well as engineering ones have also attracted numerous attentions recently. One of the most active research areas is physical science [3], especially studies of quantum many-body systems including condensed matter physics and quantum chemistry. For example, one can classify a phase of matter from its wave function [4, 5] or predict the atomization energy of molecules [6–8] from their molecular structures with sophisticated machine learning techniques.

Most of those researches employ *classical* machine learning, in which classical data are processed by classical algorithms and computers. On the other hand, there is surging interest in learning *quantum* data leveraging quantum algorithms and computers, dubbed as “quantum machine learning”, in the last few years [9–17]. This is because a primitive type of quantum computers is about to be realized in the near future, and such machines may have potentials to outperform classical ones [18, 19]. Those quantum computers in the near future are called

noisy intermediate-scale quantum (NISQ) devices [20] and consist of hundreds to thousands of physical, non-fault-tolerant qubits.

So far, quantum machine learning has been mostly applied to classical computing tasks with classical data such as pattern recognition of images [21–25]. In those studies, the classical data must be encoded in quantum states in order to be processed by quantum computers, but the encoding is generally inefficient unless there is some special structure in the data [26–28].

Therefore, it is natural to think of performing tasks with *quantum nature*. In this study, we consider the following task: predicting excited state properties of a given molecular system from its ground state wavefunction. Specifically, we are interested in the Hamiltonian for the electronic states of molecules. The question we raise and want to solve leveraging quantum machine learning is whether it is possible to predict properties of the excited states from the ground state wavefunction $|\psi_0\rangle$. According to the celebrated Hohenberg-Kohn theorem [29], one can determine an external potential for electrons and thereby the whole original electron Hamiltonian from its ground state electron density $\rho_0(r) = \langle\psi_0|\hat{r}|\psi_0\rangle$ up to constant, where \hat{r} is the position operator. Hence, it should be also possible to predict the excited states from the ground state in principle.

The task we propose here has various practical and conceptual attractions from the viewpoint of quantum machine learning and the study of quantum many-body

* hirokik@bu.edu

† nakagawa@qunasys.com

systems. First, practically, computing excited states of a given Hamiltonian needs much more computational cost and is difficult than computing the ground state [30, 31]. Since properties of the excited states are essential for thermodynamics of the system and non-equilibrium dynamics such as chemical reactions, large benefit to the study of quantum chemistry and material is expected if it is possible to predict the excited states only from the ground state. We note that applying classical machine learning to predict excited states of molecules from classical data (molecular structure, coulomb matrix, etc.) has been widely explored in the literature [32–36]. Second, the problem of encoding data to quantum computers mentioned above can be circumvented in this setup; as we will see later, it is possible to input wavefunctions into quantum computers efficiently when we consider utilizing outputs of the quantum algorithm which yields a ground state wavefunction [37]. Third, from a conceptual point of view, original “data” of quantum systems are wavefunctions, which are quantum in nature, so quantum machine learning which can treat quantum data *as they are* will take advantage of the whole information contained in the wavefunctions and potentially have a stronger predictability than classical counterparts which process only classical features of quantum data in a pure classical way [38, 39].

In this study, we propose a simple quantum machine learning scheme to predict excited state properties of the Hamiltonian of a given molecule from its ground state wavefunction. Our simulations demonstrate the potential that one can implement our model in the real NISQ devices being robust to inevitable noise of outputs in such devices. In particular, we employ and generalize the quantum reservoir computing [40] and quantum reservoir processing [41] techniques. We first mix the input wavefunctions by quantum reservoir, or the time evolution of some random Hamiltonian, and measure expectation values of simple one-qubit operators afterwards. The result of the measurements is post-processed by a classical machine learning unit and we train only the classical unit to predict target properties of the system by supervised learning, so that the number of runs of quantum computers gets small. The quantum reservoir effectively transforms the one-qubit operators into complicated multi-qubit ones which contain essential information of the system, and the classical machine learning will decode them appropriately. We numerically demonstrate the predictive power of our scheme by taking three small molecules as examples. Our model can predict the excitation energies and the transition dipole moment between the ground state and the excited state properly only from the ground state wavefunction.

The rest of the paper is organized as follows. In Sec. II, we explain our setup in detail and propose a model for quantum machine learning of excited states. We also present the way to train the model. In Sec. III, we show the result of numerical simulation of the quantum machine learning by taking several small molecules as ex-

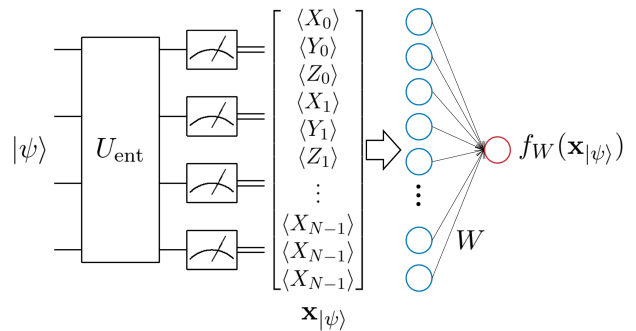


FIG. 1. Schematic diagram of our model for quantum machine learning of excited state properties of a molecule from its ground state. The input qubit state $|\psi\rangle$, which is assumed to be the ground state, is stirred by a quantum circuit U_{ent} and the measurement yields a classical vector $\mathbf{x}_{|\psi\rangle}$. A classical machine learning unit f_W with learnable parameters W outputs the target properties from $\mathbf{x}_{|\psi\rangle}$.

amples. Section IV is dedicated for the discussion of our result. We conclude the study in Sec. V.

II. METHOD

In this section, we propose a model for quantum machine learning and explain its training process. The schematic diagram of our model is described in Fig. 1.

A. Model description

Let us consider an N -qubit system and a wavefunction $|\psi\rangle \in \mathbb{C}^{2^N}$ on it. Our learning model proceeds as follows. First, an input N -qubit state $|\psi\rangle$, which is assumed to be the ground state of a given Hamiltonian here, is prepared on a quantum computer and fed into a quantum circuit which is denoted as U_{ent} in Fig 1. We call this circuit a quantum entangler or a quantum reservoir for its role of mixing quantum information of the input state $|\psi\rangle$ and encoding it to the output state $U_{\text{ent}}|\psi\rangle$. U_{ent} is chosen so as to create enough entanglement in the wavefunction and fixed for each learning task (or an experiment). The details of U_{ent} are not so important for the quality of learning as illustrated by a exactly-solvable model in Sec. IV, so one can use a quantum circuit easy to be realized in real quantum devices. After applying U_{ent} , we measure the expectation values of local Pauli operators $\{X_0, Y_0, Z_0, \dots, X_{N-1}, Y_{N-1}, Z_{N-1}\}$, where X_i, Y_i, Z_i represents a Pauli X, Y, Z operator acting on the site i . Although the total number of operators is $3N$, we can measure the operators X_0, \dots, X_{N-1} simultaneously since they commute with each other, and so can we for the cases of Y_0, \dots, Y_{N-1} and Z_0, \dots, Z_{N-1} . Hence, one can measure all operators with only three different

circuits, i.e., the number of shots of the measurement does not scale with the number of qubit N . After the measurement, we obtain a $3N$ -dimensional real-valued classical vector,

$$\begin{aligned} \mathbf{x}_{|\psi\rangle} &= (\langle X_0 \rangle, \dots, \langle Z_{N-1} \rangle)^T \\ &= \left(\langle \psi | U_{\text{ent}}^\dagger X_0 U_{\text{ent}} | \psi \rangle, \dots, \langle \psi | U_{\text{ent}}^\dagger Z_{N-1} U_{\text{ent}} | \psi \rangle \right)^T \end{aligned} \quad (1)$$

Finally, the classical data $\mathbf{x}_{|\psi\rangle}$ is fed into a classical machine learning unit with learnable parameters W , such as a linear regression model or a neural network, and the prediction $f_W(\mathbf{x}_{|\psi\rangle})$ is obtained.

We have several comments in order. First, the process to obtain $\mathbf{x}_{|\psi\rangle}$ from $|\psi\rangle$ can be viewed as compressing the data of 2^N -dimensional complex-valued vector $|\psi\rangle$ into $3N$ -dimensional real-valued data. Although the way of compression is quite complicated due to the entangler U_{ent} , the classical machine learning unit can decode the information in $\mathbf{x}_{|\psi\rangle}$ and use it to predict the properties of the excited states of the Hamiltonian. Second, the model is identical to quantum reservoir computing proposed in Ref. [40] and quantum reservoir processing proposed in Ref. [41] if we choose the linear regression as the classical machine learning unit in the model. It is also possible to consider general classical models such as the neural network, the Gaussian process regression, etc. Even though the numerical simulations we carried out in this study leverage only a linear model, which actually gives a sufficiently accurate predictions at least for the molecules we consider here, nonlinearity in the classical machine learning unit may be necessary to predict the excited states for certain tasks as discussed in Sec IV using an exactly-solvable toy model for the hydrogen molecule. Third, we stress that this scheme is suitable for one of the most promising applications of the NISQ devices, namely, the Variational Quantum Eigensolver (VQE) [37]. The VQE finds a quantum circuit which produces an approximate ground state of a given Hamiltonian by using the variational principle, and has been extended to obtain the excited states recently [42–49]. Since it can handle Hamiltonians of large systems which are intractable by classical computers, the VQE is considered as one of the best approaches to utilize the NISQ devices in the real-world problems. In our quantum machine learning model, one can use the quantum circuit obtained by the VQE to make an input state (approximate ground state wavefunction) for the training and the prediction of our model. There is no overhead cost at all to feed target data to the learning model in this case (see also Ref. [50]).

B. Supervised learning of the model

Next, we explain the procedure for supervised learning of the model. First, we define the training set \mathcal{R} whose elements r are a set of characteristics of a molecule (e.g., name of a molecule and its atomic configuration), and we

prepare the data $\{|\psi_0(r)\rangle, \mathbf{y}(r)\}_{r \in \mathcal{R}}$ for training. In the case of predicting excited states of a given Hamiltonian from its ground state, $|\psi_0(r)\rangle$ is the ground state of the molecular Hamiltonian $H(r)$ and $\mathbf{y}(r)$ contains properties of the excited states of $H(r)$, such as excitation energies. Next, by using the training set, the classical machine learning unit f_W is trained so as to predict $\{\mathbf{y}(r)\}_{r \in \mathcal{R}}$ from the classical vectors $\{\mathbf{x}_{|\psi_0(r)\rangle}\}_{r \in \mathcal{R}}$ which are calculated in the way described in the previous subsection. A typical training algorithm for the supervised learning is to minimize a cost function defined to measure the deviations of the prediction $\{f_W(\mathbf{x}_{|\psi_0(r)\rangle})\}_{r \in \mathcal{R}}$ from the training data $\{\mathbf{y}(r)\}_{r \in \mathcal{R}}$ by tuning W .

We note that our model is easier to be trained and less costly in terms of the number of runs of quantum computers compared with the so-called “quantum circuit learning” where parameters of the quantum circuit are optimized [21–24]. This is because once the classical representation of the quantum state $\{\mathbf{x}_{|\psi_0(r)\rangle}\}_{r \in \mathcal{R}}$ is obtained, there is no need to run the quantum device afterwards for training the model.

III. NUMERICAL DEMONSTRATION FOR SMALL MOLECULES

In this section, we numerically demonstrate the ability of our model to reproduce excited state properties from the ground state wavefunctions by taking small molecules as examples. We consider three types of molecules: LiH molecule, H_4 molecule whose hydrogen atoms are aligned in line with equal spacing, and H_4 molecules whose hydrogen atoms are placed on a rectangle. We call them as LiH, H_4 (line), H_4 (rectangle), respectively. We simulate our model in two situations, in one of which ideal outputs of the quantum circuits are available (*noiseless*), and in the other inevitable noise in the real NISQ devices is considered (*noisy*). The electronic ground states of those molecules with various atomic geometries are prepared by diagonalization of the Hamiltonian for the noiseless simulation and by numerically simulating the VQE for the noisy simulation. Then we train our model with the linear regression as its classical machine learning unit to predict the first and second excitation energies and the transition dipole moment among them whose values are obtained by exactly solving the Hamiltonian. Numerical results show that our model can properly reproduce the excited states and illustrate the predictive power of our model.

A. Dataset

To prepare a dataset for learning, we consider the electronic Hamiltonians of the following configurations. For LiH molecule and H_4 (line), the atomic distances are in the range of $[0.5\text{\AA}, 3.3\text{\AA}]$. For H_4 (rectangle), we choose the two spacing of atoms (lengths of two

edges) in $[0.5\text{\AA}, 2.0\text{\AA}] \times [0.5\text{\AA}, 2.0\text{\AA}]$. We perform the standard Hartree-Fock calculation by employing STO-3G minimal basis and construct the fermionic second-quantized Hamiltonian for all molecules and all configurations [51, 52] with open-source libraries PySCF [53] and OpenFermion [54]. Two Hartree-Fock orbitals with the highest and the second highest energies of LiH molecule are removed by assuming they are vacant. Then the Hamiltonian is mapped to the sum of the Pauli operators by the Jordan-Wigner transformation [55] which we denote $H(r)$. The number of qubits of the Hamiltonian for all molecules is eight.

The training and test data for learning are prepared for each Hamiltonian $H(r)$ in the following way. First, in the case of the noiseless simulation, the ground state of $H(r)$ is prepared by the exact diagonalization. In the case of the noisy simulation, the VQE algorithm [37] is applied to $H(r)$ and the approximate ground state is obtained as $|\tilde{\psi}_0(r)\rangle = U(\vec{\theta})|0\rangle$. Here $U(\vec{\theta})$ is a variational quantum circuit (ansatz) with classical parameters $\vec{\theta}$ and $|0\rangle$ is a reference state. We adapt the unitary coupled-cluster singles and doubles ansatz [37] as $U(\vec{\theta})$. Next, we compute the quantities of excited state properties to be predicted,

$$\mathbf{y}(r) = (\Delta E_1(r), \Delta E_2(r), \|\mu_{\text{eg}}(r)\|)^T, \quad (2)$$

where $\Delta E_{1(2)}(r) = E_{1(2)}(r) - E_0(r)$ is the first (second) excitation energy of $H(r)$ in the sector of neutral charge and $E_{0,1,2}(r)$ are three lowest eigenenergies of $H(r)$ in the same sector ignoring degeneracy. For our choice of the molecules and configurations, $E_0(r)$ is the energy of spin-singlet ground state S_0 , and $E_1(r)$ is the energy of the spin-triplet ground state T_0 . $E_2(r)$ is the energy of the spin-singlet excited state S_1 or the spin-triplet excited state T_1 depending on the configurations of the molecules. The transition dipole moment between the ground state and the excited state $\mu_{\text{eg}}(r)$ is defined as

$$\mu_{\text{eg}}(r) = \langle \psi_0(r) | \boldsymbol{\mu} | \psi_{\text{ex}}(r) \rangle, \quad (3)$$

where $|\psi_0(r)\rangle$ is the exact ground state of $H(r)$ (the singlet state S_0), $|\psi_{\text{ex}}(r)\rangle$ is the exact excited state of $H(r)$ which has the lowest energy among those having a non-zero transition dipole moment from the ground state (typically S_1 state), $\boldsymbol{\mu} = -e(\hat{x}, \hat{y}, \hat{z})^T$ is the dipole moment operator with electronic charge e . In this study, we use its L2-norm $\|\mu_{\text{eg}}(r)\|$ for the learning tasks. The calculation of each value of $\mathbf{y}(r)$ is performed by exact diagonalization of $H(r)$ for both noiseless and noisy simulation. We normalize those calculated values to fit them into the $[-1, 1]$ range.

In learning process, we randomly split those obtained data $\{|\tilde{\psi}_0(r)\rangle, \mathbf{y}(r)\}_r$ into a training set and a test set for the evaluation of the model. We used 30 training data points and 50 test points, respectively for the tasks of LiH and H_4 (linear) molecules, and 250 training data points and 1250 test data points, respectively for H_4 (rectangle) molecules.

B. Model for the simulations

The entangler U_{ent} in the model is chosen to be the time-evolution operator $e^{-iH_{\text{TFIM}}T}$ with the random transverse-field Ising model (TFIM),

$$H_{\text{TFIM}} = \sum_{i,j=0}^{N-1} J_{ij} Z_i Z_j + \sum_{i=0}^{N-1} h_i X_i, \quad (4)$$

where X_i and Z_j are Pauli operators acting on the site i, j -th qubit, and coefficients h_i and J_{ij} are sampled from the Gaussian distributions $N(1, 0.1)$ and $N(0.75, 0.1)$, respectively, and we set $T = 10$. These coefficients are fixed during the numerical simulation. This type of the entangler can be implemented on various types of the NISQ devices: for example, in the case of superconducting qubits it can be realized by a sequence of the cross resonance gates [56, 57] or simply tuning the resonance frequency of the qubits [21]. We note that a kind of the quantum reservoir has recently been implemented on a real NISQ device [58].

For the classical machine learning unit for numerical demonstration, we employ the linear regression (LR) [59]. Although the LR does not have nonlinearity which is in principle necessary to compute the excited state properties (see Sec. IV), it performs well enough for the molecular Hamiltonians we consider for the simulations as shown in Sec. III D, so it serves as a nice demonstrative model to evaluate the concept of our model.

The output function of the LR is

$$f^{(k)}(\mathbf{x}_{|\psi}) = \mathbf{w}_{\text{out}}^{(k)} \cdot \mathbf{x}_{|\psi}, \quad (5)$$

where $\mathbf{w}_{\text{out}}^{(k)}$ is a $3N$ -dimensional vector, or parameters of the model, to be optimized, and $k = 0, 1, 2$ corresponds to the component of the prediction for $\mathbf{y} = (y^{(0)}, y^{(1)}, y^{(2)})^T$. The model is trained to minimize the mean squared error (MSE) cost function

$$L_{\text{LR}}(\{\mathbf{w}_{\text{out}}^{(k)}\}) = \frac{1}{3|\mathcal{R}|} \sum_{r \in \mathcal{R}} \sum_{k=0}^2 \left| \mathbf{w}_{\text{out}}^{(k)} \cdot \mathbf{x}_{|\psi_0(r)} - y(r)^{(k)} \right|^2, \quad (6)$$

where \mathcal{R} represents the training dataset. The exact optimum of the cost function can be obtained as

$$\mathbf{w}_{\text{out}}^{(k)*} = (V^T V)^{-1} V^T \mathbf{Y}^{(k)}, \quad (7)$$

where V is a $|\mathcal{R}| \times 3N$ dimensional matrix whose i -th row is $\mathbf{x}_{|\psi_0(r_i)}^T$, and $\mathbf{Y}^{(k)}$ is a $|\mathcal{R}|$ dimensional column vector whose i -th component is $y(r_i)^{(k)}$, where r_i is the i -th element of \mathcal{R} . The whole classical process requires the time complexity of $\mathcal{O}(N^3 + N^2|\mathcal{R}|)$.

C. Simulation of quantum circuits

To check the practical advantage of our model with the NISQ devices, we numerically simulate quantum circuits of the model (including preparation of the ground

state wavefunctions by the VQE) considering noiseless and noisy situations. The latter reflects a more realistic situation for experiments, but we stress that the former still serves as a reference point to judge whether the model has capability of performing the learning task or not.

In the noiseless simulation, the expectation value of the Pauli operator $\langle \psi | P_i | \psi \rangle$, where the $|\psi\rangle$ is a quantum state and P_i is the Pauli operator acting on i -th qubit, is estimated exactly by calculating the inner product. In the noisy simulation, we consider two error sources which make estimations of those expectation values deviate from the exact ones. One of them is a sequence of the depolarizing noise channels [60] that transform the quantum state $\rho = U_{\text{ent}} |\psi\rangle \langle \psi| U_{\text{ent}}^\dagger$ from the reservoir into $\rho' = \mathcal{E}_{N-1} \circ \dots \circ \mathcal{E}_0(\rho)$, where \mathcal{E}_i is the depolarizing channel that acts as $\mathcal{E}(\sigma) = (1-p)\sigma + \frac{p}{3}(X_i\sigma X_i + Y_i\sigma Y_i + Z_i\sigma Z_i)$. We take $p = 0.01$ in the simulation. The other source is the so-called shot noise that stems from the finite number of shots in the projective measurements of the Pauli operator P_i . Each measurement returns ± 1 according to the probability distribution determined by the exact values of $\text{Tr}(\rho' P_i)$. We sample 10^6 shots of measurements for each Pauli operator, which is still feasible number in experiments [56].

D. Results

The model described in the previous subsections is trained by the training dataset and evaluated by the test set. The evaluation is performed based on the mean absolute error (MAE) for the test set \mathcal{T} ,

$$C_{\mathcal{T}} = \frac{1}{3|\mathcal{T}|} \sum_{r \in \mathcal{T}} \sum_{k=0}^2 |\mathbf{f}_W(\mathbf{x}_{|\psi_0(r)}) - \mathbf{y}(r)^{(k)}|, \quad (8)$$

where $\mathbf{f}_W(\mathbf{x})$ is the output of the model considered as a vector. We train and evaluate the model for each molecule separately.

1. Noiseless simulation

The prediction results by the trained model in the noiseless numerical simulation are shown in Figs. 2 and 3. Clearly, our model reproduces the exact values of the excited state properties $\mathbf{y}(r)$ for all of the three molecule types. In addition, we also investigate the necessity of the entangler U_{ent} by comparing the values of the MAE for the test set (Eq. (8)) after the learning. The evaluations of the learners with and without the entangler are summarized in Table I, indicating that the entangler significantly enhances the predictive power of the model. In Sec. IV, another supporting result for the necessity of the entangler is presented by using an exactly solvable model for the hydrogen molecule.

These results from the noiseless simulations illustrate the predictive power of our model for the difficult task to predict the excited state properties only from the ground state.

2. Noisy simulation

In order to evaluate our scheme in a realistic situation with a quantum device, we add two noise sources to the simulation as described in Sec. III C. In this case, in order to increase the noise robustness, we make two modifications to the noiseless case as follows. First, after obtaining the classical vectors $\{\mathbf{x}_{|\psi_0(r)}\}_{r \in \mathcal{R}}$ by processing the training dataset with the noisy quantum circuit, we make 100 copies of every vector $\mathbf{x}_{|\psi_0(r)}$ on a classical computer, and add a gaussian noise $N(0, 2 \times 10^{-3})$ to each component of it. We stack these vectors, and now we have a new $100|\mathcal{R}| \times 3N$ dimensional matrix V' . The vector $\mathbf{Y}^{(k)}$ is also duplicated 100 times to match up with V' (let us call this new vector $\mathbf{Y}'^{(k)}$ for later use). Notice that this modification does not affect the required number of measurements of the quantum circuit. Second, we add the L2 regularization term into the cost function of the LR, specifically,

$$L'_{\text{LR}}(\{\mathbf{w}_{\text{out}}^{(k)}\}) = L_{\text{LR}}(\{\mathbf{w}_{\text{out}}^{(k)}\}) + \alpha \|\mathbf{w}_{\text{out}}^{(k)}\|^2, \quad (9)$$

where we used $\alpha = 10^{-3}$ in the simulations. We may obtain the exact optimum by computing

$$\mathbf{w}_{\text{out}}^{(k)*} = (V'^T V')^{-1} V'^T \mathbf{Y}'^{(k)} + \alpha I, \quad (10)$$

where I is an identity matrix of $3N \times 3N$ dimensions. Both of these two modifications are kinds of regularizations preventing the model from overfitting due to the outliers with large noises.

The prediction results are presented in Figs. 4 and 5. We see that the model still predicts $\mathbf{y}(r)$ well even in this noisy case.

IV. DISCUSSION

A. Necessity of the entangler U_{ent} and the nonlinearity of f_W

Here we discuss the necessity of the entangler U_{ent} and the nonlinearity in the classical machine learning unit f_W by considering an exactly solvable model of fermions, namely, the 2-site fermion Hubbard model at half-filling [61].

The 2-site Hubbard model is defined by

$$H_{\text{Hub}}(U) = - \sum_{\sigma=\uparrow,\downarrow} \left(c_{0,\sigma}^\dagger c_{1,\sigma} + \text{h.c.} \right) + U \sum_{i=0,1} n_{i,\uparrow} n_{i,\downarrow} \quad (11)$$

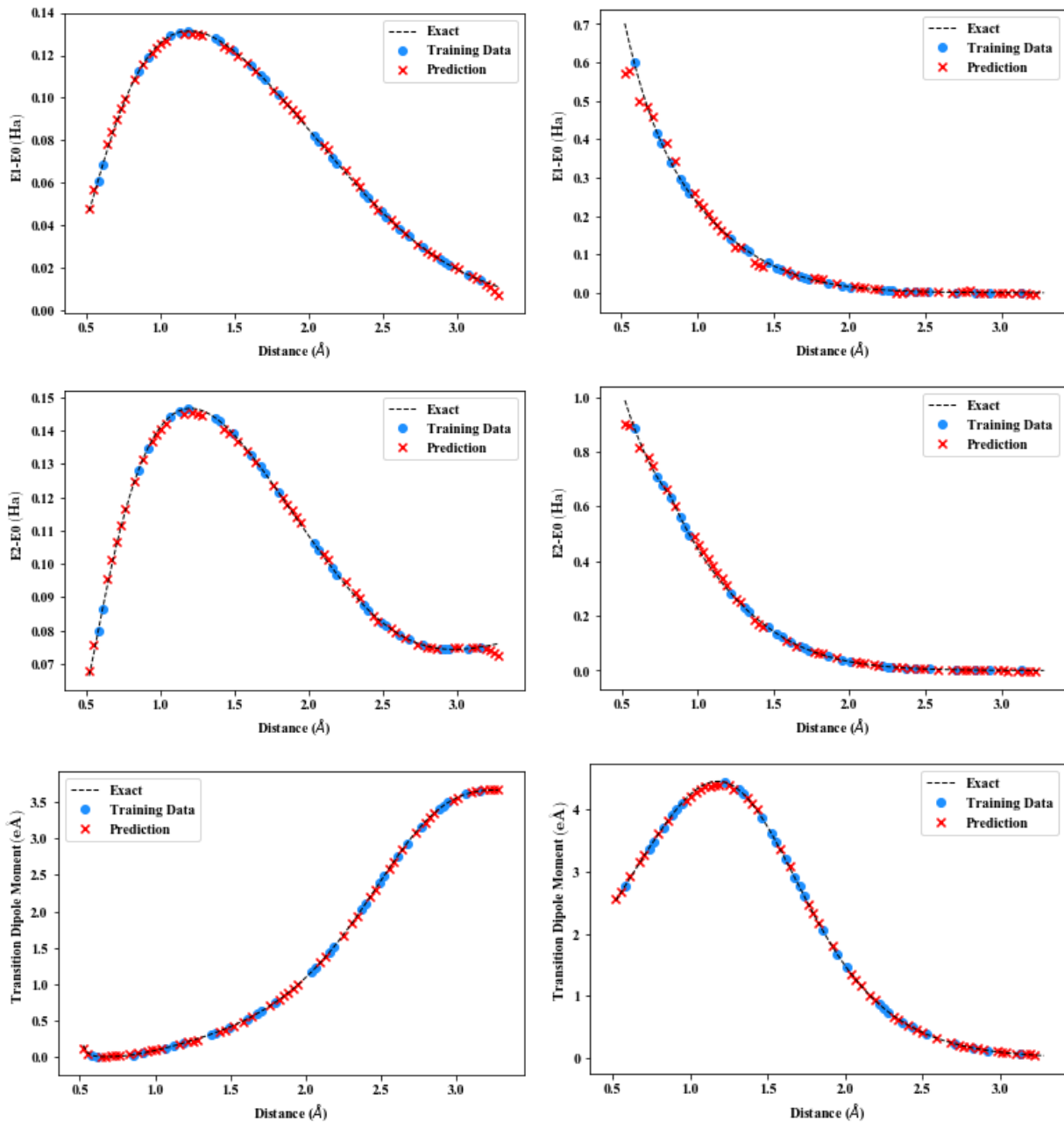


FIG. 2. The prediction results by the trained model for LiH (left column) and H₄ (line) (right column) for the noiseless simulations. Top, middle, and bottom panels display the first, second excitation energies and the transition amplitude, respectively. The blue circles indicate the training data points and the red ones do the predictions. The exact values are displayed as the black line.

	LiH	H4 (line)	H4 (rectangle)
Test MAE with entangler U_{ent}	0.0181	0.0203	0.0836
Test MAE without entangler U_{ent}	0.172	0.324	0.300
Random Guess	0.673	0.544	0.444

TABLE I. The MAEs evaluated with the test set for the trained models in the noiseless situation with and without the entangler. The output values and the excited state properties are rescaled in the $[-1, 1]$ range. The MAEs for the random guess are also presented as a reference.

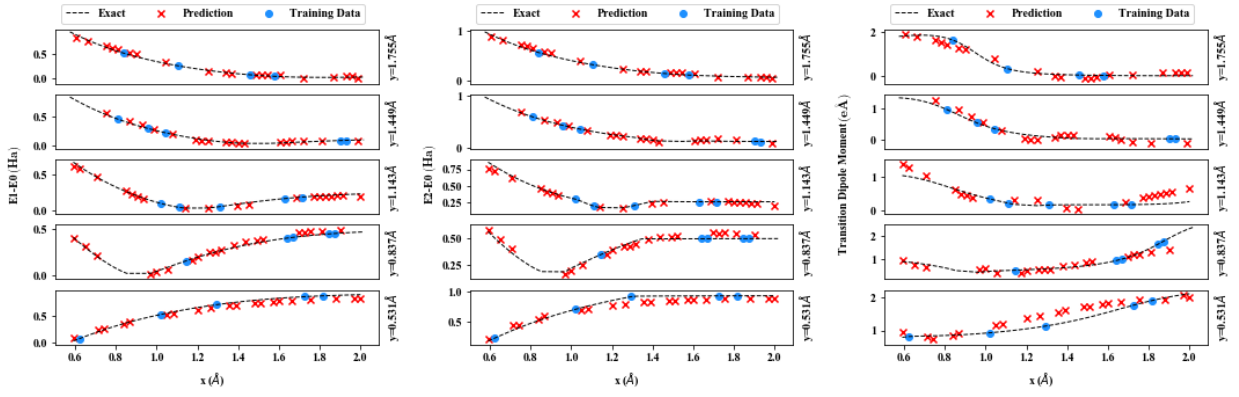


FIG. 3. The same figures as Fig. 2 for H_4 (rectangle). x and y denote the two atomic spacings of the rectangular geometry.

where $c_{i,\sigma}, c_{i,\sigma}^\dagger$ are fermionic creation and annihilation operators acting on an electron with spin $\sigma = \uparrow, \downarrow$ located at i -th site ($i = 0, 1$), and $n_{i,\sigma} = c_{i,\sigma}^\dagger c_{i,\sigma}$ is the number operator of an electron with spin σ at i -th site. The parameter $U > 0$ determines the strength of electron repulsion. This system can be considered as a simplified model of the hydrogen molecule whereas it also serves as a prototype of strongly-correlated materials. When we restrict ourselves into the sector where the number of electrons is two, or focus on the neutral hydrogen states, the first and second excitation energies are

$$\Delta E_1 = \frac{U}{2} \left(-1 + \sqrt{1 + \frac{16}{U^2}} \right), \quad (12)$$

$$\Delta E_2 = \frac{U}{2} \left(1 + \sqrt{1 + \frac{16}{U^2}} \right), \quad (13)$$

respectively.

Applying the Jordan-Wigner transformation [55] to the system (11), we obtain the 4-qubit Hamiltonian $H_{\text{qubit}}(U)$. We denote the ground state of $H_{\text{qubit}}(U)$ as $|\psi_0(U)\rangle$. When there is no entangler, the classical vector $\mathbf{x}_{|\psi_0(U)\rangle}$ is trivial because

$$\langle X_j \rangle_{\text{GS}} = \langle Y_j \rangle_{\text{GS}} = \langle Z_j \rangle_{\text{GS}} = 0 \quad (14)$$

holds for all qubit sites $j = 0, 1, 2, 3$, where we define $\langle \psi_0(U) | \dots | \psi_0(U) \rangle$ as $\langle \dots \rangle_{\text{GS}}$. In contrast, when there is an entangler U_{ent} in our model, it converts the Pauli operators X_j, Y_j, Z_j into a sum of more complicated Pauli strings like $U_{\text{ent}}^\dagger Z_0 U_{\text{ent}} = Z_0 Z_1 + 0.2 Z_1 X_1 Z_2 Y_2 + \dots$ in the Heisenberg picture. Therefore the classical vector $\mathbf{x}_{|\psi_0(U)\rangle}$ contains contributions from the terms like $\langle Z_0 Z_1 \rangle_{\text{GS}}$. It follows that

$$\langle Z_0 Z_1 \rangle_{\text{GS}} = - \left(1 + \frac{16}{U^2} \right)^{-1/2}, \quad (15)$$

and

$$\Delta E_1 = \frac{2(1 + \langle Z_0 Z_1 \rangle_{\text{GS}})}{\sqrt{1 - \langle Z_0 Z_1 \rangle_{\text{GS}}^2}}, \quad (16)$$

$$\Delta E_2 = \frac{2(1 - \langle Z_0 Z_1 \rangle_{\text{GS}})}{\sqrt{1 - \langle Z_0 Z_1 \rangle_{\text{GS}}^2}}. \quad (17)$$

These equations indicate that the excitation energies can be predicted by utilizing the values of $\langle Z_0 Z_1 \rangle_{\text{GS}}$ appropriately. Therefore, one can see that it is possible to predict the excitation energies from the classical vector $\mathbf{x}_{|\psi_0(U)\rangle}$ if there is the entangler and the nonlinearity in the classical machine learning unit f_W . These equations also imply that the details of the entangler, which determine coefficients of the terms like $\langle Z_0 Z_1 \rangle_{\text{GS}}$ in $\mathbf{x}_{|\psi_0(U)\rangle}$, is not so important for predictions; the classical machine learning unit can compensate difference of such coefficients.

B. Generalizability

In the numerical simulations in Sec. III, the models are trained and evaluated for each molecule separately. The generalizability of our model to predict properties of various molecules simultaneously is one possibility of our model for future extensions.

To make our model more powerful and capable of inputting various molecules, several modifications can be considered. First, including the ground state energy which can also be calculated by the VQE besides the ground state in the input of the classical machine learning unit f_W will be necessary since it can determine the energy scale of an input molecule. Second, replacing the entangler U_{ent} with a parametrized quantum circuit $V(\theta)$ and optimizing the circuit parameters θ along with the classical machine learning unit increase the degree of freedoms of the model and may result in a better predictive power, with a possible drawback that the number of required experiments on the NISQ devices would increase

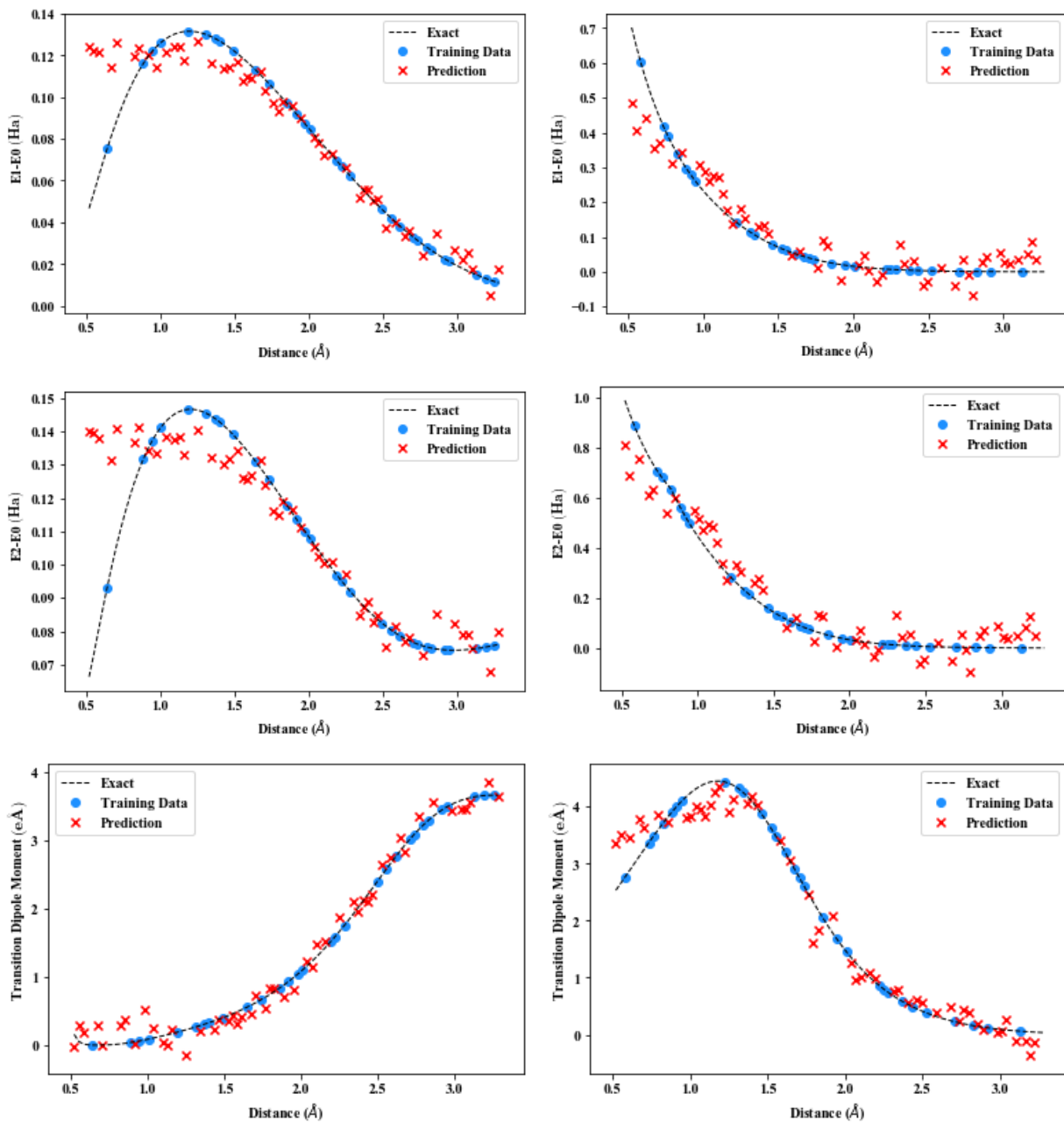


FIG. 4. The prediction results by the trained model for LiH (left column) and H_4 (line) (right column) for the noisy simulations. Top, middle, and bottom panels display the first, second excitation energies and the transition amplitude, respectively. The blue circles indicate the training data points and the red ones do the predictions. The exact values are displayed as the black line.

in the training step. Exploring these ideas is an interesting future direction of the work.

V. CONCLUSION

In this study, we introduce a new quantum machine learning framework for predicting excited state properties of a molecule from its ground state wavefunction.

By employing the quantum reservoir and choosing simple one-qubit observables for measurements accompanied by post-processing with the classical machine learning, one may process our framework easily on the NISQ devices requiring the realistic number of runs of them. The numerical simulations with and without the noise in outputs of quantum circuits demonstrate that our model accurately predicts the excited states. Although our framework is tested only with small molecules to illustrate its poten-

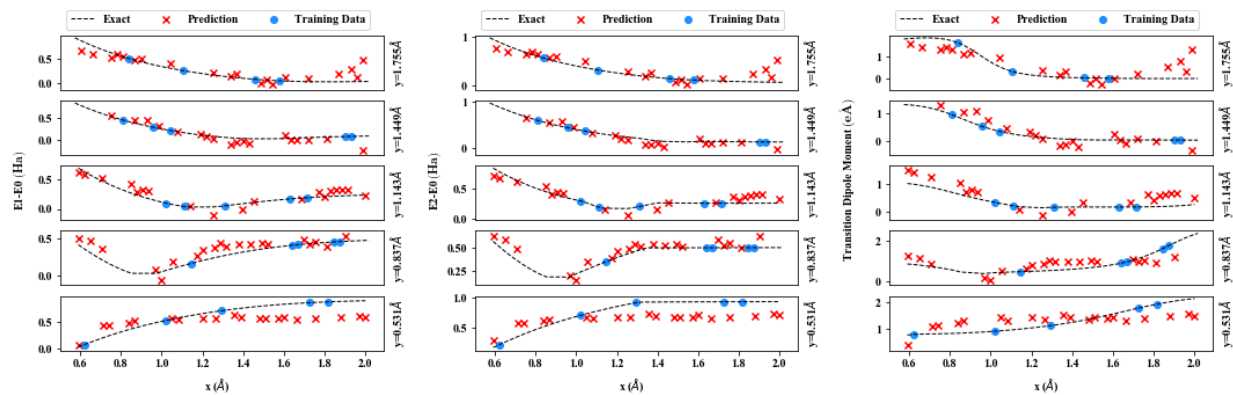


FIG. 5. The same figures as Fig. 4 for H_4 (rectangle). x and y denote two atomic spacings of the rectangular geometry.

tial in the numerical simulations, we expect that it will benefit calculation of excited states of larger molecules by reducing the computational cost from calculating exact solutions. Our result opens up further possibility to utilize the NISQ devices in the study of quantum chemistry and quantum material fields.

ACKNOWLEDGEMENT

HK was supported by QunaSys Inc. HK and YON acknowledges Suguru Endo, Kosuke Mitarai, Nobuyuki Yoshioka, Wataru Mizukami, and Keisuke Fujii for valuable discussions. This work was also supported by MEXT Q-LEAP JPMXS0118068682.

-
- [1] Y. LeCun, Y. Bengio, and G. Hinton, *Nature* **521**, 436 (2015).
- [2] I. Goodfellow, Y. Bengio, and A. Courville, *Deep Learning* (MIT Press, 2016).
- [3] G. Carleo, I. Cirac, K. Cranmer, L. Daudet, M. Schuld, N. Tishby, L. Vogt-Maranto, and L. Zdeborová, *Rev. Mod. Phys.* **91**, 045002 (2019).
- [4] J. Carrasquilla and R. G. Melko, *Nature Physics* **13**, 431 (2017).
- [5] E. P. L. van Nieuwenburg, Y.-H. Liu, and S. D. Huber, *Nature Physics* **13**, 435 (2017).
- [6] M. Rupp, A. Tkatchenko, K.-R. Müller, and O. A. von Lilienfeld, *Phys. Rev. Lett.* **108**, 058301 (2012).
- [7] G. Montavon, K. Hansen, S. Fazli, M. Rupp, F. Biegler, A. Ziehe, A. Tkatchenko, A. V. Lilienfeld, and K.-R. Müller, in *Advances in Neural Information Processing Systems 25*, edited by F. Pereira, C. J. C. Burges, L. Bottou, and K. Q. Weinberger (Curran Associates, Inc., 2012) pp. 440–448.
- [8] K. Hansen, G. Montavon, F. Biegler, S. Fazli, M. Rupp, M. Scheffler, O. A. von Lilienfeld, A. Tkatchenko, and K.-R. Müller, *Journal of Chemical Theory and Computation*, *Journal of Chemical Theory and Computation* **9**, 3404 (2013).
- [9] A. W. Harrow, A. Hassidim, and S. Lloyd, *Phys. Rev. Lett.* **103**, 150502 (2009).
- [10] N. Wiebe, D. Braun, and S. Lloyd, *Phys. Rev. Lett.* **109**, 050505 (2012).
- [11] S. Lloyd, M. Mohseni, and P. Rebentrost, *Nature Physics* **10**, 631 (2014).
- [12] P. Rebentrost, M. Mohseni, and S. Lloyd, *Phys. Rev. Lett.* **113**, 130503 (2014).
- [13] M. Schuld, I. Sinayskiy, and F. Petruccione, *Phys. Rev. A* **94**, 022342 (2016).
- [14] I. Kerenidis and A. Prakash, arXiv:1704.04992 (2017).
- [15] G. Wang, *Phys. Rev. A* **96**, 012335 (2017).
- [16] J. Biamonte, P. Wittek, N. Pancotti, P. Rebentrost, N. Wiebe, and S. Lloyd, *Nature* **549**, 195 (2017).
- [17] I. Cong, S. Choi, and M. D. Lukin, *Nature Physics* **15**, 1273 (2019).
- [18] A. W. Harrow and A. Montanaro, *Nature* **549**, 203 (2017).
- [19] F. Arute, K. Arya, R. Babbush, D. Bacon, J. C. Bardin, R. Barends, R. Biswas, S. Boixo, F. G. S. L. Brandao, D. A. Buell, B. Burkett, Y. Chen, Z. Chen, B. Chiaro, R. Collins, W. Courtney, A. Dunsworth, E. Farhi, B. Foxen, A. Fowler, C. Gidney, M. Giustina, R. Graff, K. Guerin, S. Habegger, M. P. Harrigan, M. J. Hartmann, A. Ho, M. Hoffmann, T. Huang, T. S. Humble, S. V. Isakov, E. Jeffrey, Z. Jiang, D. Kafri, K. Kechedzhi, J. Kelly, P. V. Klimov, S. Knysh, A. Korotkov, F. Kostritsa, D. Landhuis, M. Lindmark, E. Lucero, D. Lyakh, S. Mandrà, J. R. McClean, M. McEwen, A. Megrant, X. Mi, K. Michielsen, M. Mohseni, J. Mutus, O. Naaman, M. Neeley, C. Neill, M. Y. Niu, E. Ostby, A. Petukhov, J. C. Platt, C. Quintana, E. G. Rieffel, P. Roushan, N. C. Rubin, D. Sank, K. J. Satzinger, V. Smelyanskiy, K. J. Sung, M. D. Trevithick, A. Vainsencher, B. Villalonga, T. White, Z. J. Yao, P. Yeh, A. Zalcman, H. Neven, and J. M. Martinis, *Nature* **574**, 505 (2019).
- [20] J. Preskill, *Quantum* **2**, 79 (2018).
- [21] V. Havlíček, A. D. Córcoles, K. Temme, A. W. Harrow, A. Kandala, J. M. Chow, and J. M. Gambetta, *Nature* **567**, 209 (2019).

- [22] T. Kusumoto, K. Mitarai, K. Fujii, M. Kitagawa, and M. Negoro, arXiv:1911.12021 (2019).
- [23] K. Mitarai, M. Negoro, M. Kitagawa, and K. Fujii, *Phys. Rev. A* **98**, 032309 (2018).
- [24] E. Farhi and H. Neven, arXiv:1802.06002 (2018).
- [25] C. Wilson, J. Otterbach, N. Tezak, R. Smith, G. Crooks, and M. da Silva, arXiv:1806.08321 (2018).
- [26] V. Giovannetti, S. Lloyd, and L. Maccone, *Phys. Rev. Lett.* **100**, 160501 (2008).
- [27] V. Giovannetti, S. Lloyd, and L. Maccone, *Phys. Rev. A* **78**, 052310 (2008).
- [28] A. Prakash, *Quantum algorithms for linear algebra and machine learning.*, Ph.D. thesis, UC Berkeley (2014).
- [29] P. Hohenberg and W. Kohn, *Phys. Rev.* **136**, B864 (1964).
- [30] B. O. Roos, *Lecture Notes in Quantum Chemistry: European Summer School in Quantum Chemistry*, Vol. 58 (Springer Science & Business Media, 2012).
- [31] T. Helgaker, P. Jorgensen, and J. Olsen, *Molecular electronic-structure theory* (John Wiley & Sons, 2014).
- [32] G. B. Goh, N. O. Hodas, and A. Vishnu, *Journal of Computational Chemistry* **38**, 1291 (2017).
- [33] G. Montavon, M. Rupp, V. Gobre, A. Vazquez-Mayagoitia, K. Hansen, A. Tkatchenko, K.-R. Müller, and O. A. von Lilienfeld, *New Journal of Physics* **15**, 095003 (2013).
- [34] R. Ramakrishnan, M. Hartmann, E. Tapavicza, and O. A. von Lilienfeld, *The Journal of Chemical Physics* **143**, 084111 (2015).
- [35] F. Häse, S. Valleau, E. Pyzer-Knapp, and A. Aspuru-Guzik, *Chemical science* **7**, 5139 (2016).
- [36] Z. Wu, B. Ramsundar, E. Feinberg, J. Gomes, C. Geniesse, A. S. Pappu, K. Leswing, and V. Pande, *Chem. Sci.* **9**, 513 (2018).
- [37] A. Peruzzo, J. McClean, P. Shadbolt, M.-H. Yung, X.-Q. Zhou, P. J. Love, A. Aspuru-Guzik, and J. L. O’Brien, *Nature Communications* **5**, 4213 (2014).
- [38] M. Sasaki, A. Carlini, and R. Jozsa, *Phys. Rev. A* **64**, 022317 (2001).
- [39] M. Sasaki and A. Carlini, *Phys. Rev. A* **66**, 022303 (2002).
- [40] K. Fujii and K. Nakajima, *Phys. Rev. Applied* **8**, 024030 (2017).
- [41] S. Ghosh, A. Opala, M. Matuszewski, T. Paterek, and T. C. H. Liew, *npj Quantum Information* **5**, 35 (2019).
- [42] J. R. McClean, M. E. Kimchi-Schwartz, J. Carter, and W. A. de Jong, *Phys. Rev. A* **95**, 042308 (2017).
- [43] J. I. Colless, V. V. Ramasesh, D. Dahlen, M. S. Blok, M. E. Kimchi-Schwartz, J. R. McClean, J. Carter, W. A. de Jong, and I. Siddiqi, *Phys. Rev. X* **8**, 011021 (2018).
- [44] K. M. Nakanishi, K. Mitarai, and K. Fujii, *Phys. Rev. Research* **1**, 033062 (2019).
- [45] R. M. Parrish, E. G. Hohenstein, P. L. McMahon, and T. J. Martínez, *Phys. Rev. Lett.* **122**, 230401 (2019).
- [46] O. Higgott, D. Wang, and S. Brierley, *Quantum* **3**, 156 (2019).
- [47] T. Jones, S. Endo, S. McArdle, X. Yuan, and S. C. Benjamin, *Phys. Rev. A* **99**, 062304 (2019).
- [48] P. J. Ollitrault, A. Kandala, C.-F. Chen, P. K. Barkoutsos, A. Mezzacapo, M. Pistoia, S. Sheldon, S. Woerner, J. Gambetta, and I. Tavernelli, arXiv preprint arXiv:1910.12890 (2019).
- [49] J. Tilly, G. Jones, H. Chen, L. Wossnig, and E. Grant, arXiv:2001.04941 (2020).
- [50] A. Uvarov, A. Kardashin, and J. Biamonte, arXiv:1906.10155 (2019).
- [51] S. McArdle, S. Endo, A. Aspuru-Guzik, S. Benjamin, and X. Yuan, arXiv:1808.10402 (2018).
- [52] Y. Cao, J. Romero, J. P. Olson, M. Degroote, P. D. Johnson, M. Kieferová, I. D. Kivlichan, T. Menke, B. Peropadre, N. P. D. Sawaya, S. Sim, L. Veis, and A. Aspuru-Guzik, *Chemical Reviews* **119**, 10856 (2019).
- [53] Q. Sun, T. C. Berkelbach, N. S. Blunt, G. H. Booth, S. Guo, Z. Li, J. Liu, J. D. McClain, E. R. Sayfutyarova, S. Sharma, S. Wouters, and G. K. Chan, “Pyscf: the pythonbased simulations of chemistry framework,” (2017).
- [54] J. R. McClean, K. J. Sung, I. D. Kivlichan, Y. Cao, C. Dai, E. S. Fried, C. Gidney, B. Gimby, P. Gokhale, T. Haner, T. Hardikar, V. Havlíček, O. Higgott, C. Huang, J. A. Izaac, Z. J. W. Jiang, X. Liu, S. McArdle, M. Neeley, T. O’Brien, B. O’Gorman, I. Ozfidan, M. D. Radin, J. Romero, N. C. Rubin, N. P. D. Sawaya, K. Setia, S. Sim, D. S. Steiger, M. Steudtner, Q. Sun, W. Sun, D. Wang, F. Zhang, and R. Babbush (2017) arXiv:1710.07629.
- [55] P. Jordan and E. Wigner, *Zeitschrift für Physik* **47**, 631 (1928).
- [56] A. Kandala, A. Mezzacapo, K. Temme, M. Takita, M. Brink, J. M. Chow, and J. M. Gambetta, *Nature* **549**, 242 (2017).
- [57] A. Kandala, K. Temme, A. D. Córcoles, A. Mezzacapo, J. M. Chow, and J. M. Gambetta, *Nature* **567**, 491 (2019).
- [58] J. Chen, H. I. Nurdin, and N. Yamamoto, arXiv:2001.09498 (2020).
- [59] C. M. Bishop, *Pattern recognition and machine learning*, Information science and statistics (Springer, New York, NY, 2006).
- [60] M. A. Nielsen and I. L. Chuang, *Quantum Computation and Quantum Information: 10th Anniversary Edition*, 10th ed. (Cambridge University Press, New York, NY, USA, 2011).
- [61] J. Hubbard and B. H. Flowers, *Proceedings of the Royal Society of London. Series A. Mathematical and Physical Sciences* **276**, 238 (1963).